Published in Materials Science and Engineering: A
Volumes 460-461, 15 July 2007, Pages 111-120

http://dx.doi.org/10.1016/j.msea.2007.01.080

Synthesis and Characterization of Silicon Carbide by Reaction Milling in a Dual-drive Planetary Mill

Debasis Chaira, B.K. Mishra∗ and S. Sangal

Department of Materials and Metallurgical Engineering
Indian Institute of Technology Kanpur

∗ Regional Research Laboratory
Council of Scientific & Industrial Research
Bhubaneswar, India

Abstract

The formation of silicon carbide from elemental silicon and graphite powder by reaction milling in a specially designed dual drive planetary mill is reported. The phase

evolutions, particle size distribution, and morphology of particles during milling are studied during a 40-hour grinding period. X-ray diffraction study indicates complete conversion of silicon and graphite to silicon carbide. The crystallite size varies from 150 nm from the start to 10 nm after 40 hours of milling. The lattice strain increases with milling up to about 20 hours when SiC forms and subsequently with the formation of SiC it is reduced.

Al-SiC composites are prepared by mixing Al with 40 hours milled final SiC powder and sintered in an inert atmosphere. The composites show excellent compatibility between Al and SiC particles, no voids or cracks are present.

Keywords: Dual drive planetary mill, reaction milling, and silicon carbide.

1. INTRODUCTION

Metal carbides possess unusual properties that make them desirable and useful engineering materials for many industrial applications. They have great hardness, high melting points (2000°C- 3000°C). One important property of the metal carbides is their chemical stability at room temperature and these are unique in that they combine the characteristic properties of metals and ceramics. The properties of metal carbides place them on top of industrials applications. In the industrial scale of production, the technique of powder metallurgy is usually used for preparing metal carbides. In this process, a direct reaction between the metal powder and graphite takes place at extremely high temperatures. The higher cost of high temperature processing increases the price of end product which is considered a major disadvantage in developing countries.

Silicon carbide is a promising material used in electronic devices that are particularly used at high temperatures. This is due to its high temperature electrical properties, high breakdown voltage, and high electron mobility. It is also used in various types of high temperature applications such as heating elements and refractory material for furnaces due to its high fracture strength, excellent wear and creep resistance, high resistance to corrosion, good thermal conductivity and relatively low coefficient of thermal expansion. It is also a good filler material owing to its thermal and chemical stability. This is valid both during synthesis and under severe service conditions.

Silicon carbide can be produced by many methods (Vogt, et al., 1985 [1]; Canon et al., 1982 [2, 3]). The traditional method which is to a large extent commercialized is known as the Acheson process. Here a solid-state reaction between sand and petroleum coke at very high temperature (2500°C) leads to the formation of silicon carbide. The commercial product has a large grain size and is invariably contaminated with oxygen. The other fabrication processes for obtaining SiC include polymer pyrolysis, chemical vapor deposition (CVD) and even hot pressing. Liquid phase reactions have also been used to synthesize silicon carbide, as reported by Ritter (1995) [4]. Most of the abovementioned approaches require temperature higher than 1500°C. However, silicon carbide can also be synthesized without heating, such as high energy milling of elemental powders at ambient temperature, which is termed as reaction milling.

The reaction milling or mechano-chemical synthesis of metal carbides was proposed by Le Caer et al. (1990) [5]. They prepared carbides of Ti, V, Cr, Mn, Fe, Co, Ni, Zr, Nb, Mo, Ta, W, Re, Al, and Si by milling the above elements with graphite powder in either a SPEX 8000 shaker mill or a Fritsch P-7 planetary mill for a fixed amount of time

(Matteazzi and Caer, 1991) [6]. El-Eskandarany et al. (1995) [7] prepared stoichiometric SiC powders by solid-state reaction of elemental silicon and carbon powders via the room temperature mechanical alloying process. Complete fcc–SiC alloy powders were obtained after 300 hours of milling. The mechanical alloying process was performed in a high-energy ball mill. Yang and Shaw (1996) [8] also produced SiC from silicon and graphite by attrition milling. Based on the x-ray line broadening they concluded that product compound was β-SiC where the average crystallite size was of the order of 70 nm.

2. REACTION MILLING

Reaction milling is a process where simultaneous milling and chemical reaction takes place in a highly energetic environment. It can be practiced in planetary mills where the force field could be made to vary from one to two orders of magnitude compared to equivalent size ball mills. Reaction milling uses mechanical processing to induce chemical reactions. The major areas where reaction milling could be applied include ultrafine powder production, mineral and waste processing, metals refining, combustion reactions, production of a fine dispersion of second phase particles, extension of solubility limits, refinement of the matrix microstructure/nanograin formation, formation of amorphous phases. An important feature of reaction milling is the refinement of microstructure (i.e., grain size and particle size) associated with simultaneous particle deformation, fracture, and welding processes that accompany ball/powder collision events. The energy transmitted to crystalline powders during milling may result in dislocation cell structure that develops into random nanostructured grains with increasing

milling time. It should be realized that even though nanometer grain sizes are realized during mechano-chemical processing, the particle size typically decreases only to micrometer level.

Planetary milling can induce chemical reactions in a variety of powder mixtures. In fact it has been shown that mechanical activation substantially increases the kinetics of solid-state chemical reactions (Schwarz and Petrich, 1988 [9]; Schwarz et al., 1985 [10]). In the systems of interest here, reaction does not occur at the beginning of the milling process. However, it becomes possible after a certain activation time, as milling reduces the particle size, thoroughly mixes the components, and increases the number of chemically active defect sites. The activated states or the reaction zones not only increase as particle and grain sizes decrease, but are also regenerated through the repeated particle fracture and welding events. As a consequence, reactions that require high temperatures to occur will occur at low temperatures in a planetary mill without any need for external heating. Thus, a wide range of chemical reactions can be mechanically initiated.

3. MILL/MEDIA MECHANICS

Planetary mills are extensively used for ultra fine grinding and synthesis of advanced materials. The gravity field becomes an important limiting factor in conventional ball mills, as the energy in these kinds of mills is very small. The planetary mill overcomes the limitation of the gravitational field, supplying a strong acceleration field. This type of mill has been used not only for grinding but also for mechanical alloying (MA) and mechanochemical (MC) operations (McCormick and Froes, 1998) [11]. The dual drive planetary mill consists of a gyratory shaft and two cylindrical steel jars, both are rotated

simultaneously and separately at high speed. Such high-speed rotation of both jars and the shaft makes the balls to move strongly and violently, leading to large impact energy of balls that improves the grinding performance. The dual drive planetary mill developed specifically for the synthesis of nanocarbides has a rotating shaft that sweeps a circle of diameter 750 mm. The two steel jars of 13.5 cm diameter (2500 ml each) rotate about their own axes around the common axis of the main shaft. The planetary mill is powered by two motors—one 5 HP motor works on the main rotating shaft and another 3 HP motor drives the jars. The rotating speed of both motors can be varied independently and continuously by a frequency controller. This mill design follows closely the patented design of Rajamani et al. (1990) [12] with several minor modifications to improve its performance and suit to the local conditions.

Figure 1 shows a configuration of one half of the planetary mill where a jar rotates about a primary axis O. Here G is the diameter of rotation of the axis of the jar and D is the diameter of the jar itself. Once these parameters are fixed, it turns out, that the planetary mill could be simply characterized by the ratio of the diameter of rotation of the mill axis G to the diameter of the mill D. Let R be the ratio of speed of rotation of the mill axis to the speed of rotation of the mill about its center. Then, if the shaft rotates at an angular velocity of ω, the mill rotates at $R\omega$ on the shaft. A negative value of R indicates that the mill and the shaft rotate in opposite direction. During operation, four different kinds of forces act on a ball inside any one of the jars as shown in Fig. 1. These are (i) centrifugal force about the fixed gyrating axes, (ii) centrifugal force about the mill axis,

(iii) Coriolis force due to the planetary motion (rotating coordinate system). These forces produce a special acceleration field inside the mill which is difficult to visualize.

The dynamics of the planetary mill dictates that

$$R = -1 \pm \sqrt{\frac{G}{D}}$$

which allows computation of the critical speed. The percent critical speed is

$$\%CS = \frac{N_2}{R \times N_1} \times 100$$

where N_1 is the gyrating speed and N_2 is the jar speed. In our case, the mill was operated at 63% critical speed. This was arrived by doing the following calculation:

$$R = -1 \pm \sqrt{\frac{750}{135}} = -1 \pm 2.36$$

Taking the minus sign for opposite direction of motion between the jar and the main shaft it can be shown that

$$R = -3.36$$

The percent critical speed is calculated by considering the shaft speed and jar speed as 225 and 475 rpm. Therefore

$$\%CS = \frac{475}{3.36 \times 225} \times 100 = 62.8$$

3.1. Motion analysis

The mechanical description of the milling process is best understood by considering the overall motion of the balls inside the milling chamber and the mechanics of an individual collision including the elastic and plastic deformation of the powder. Much research along these lines was performed in connection with modeling the mechanical

alloying process and a summary of this research is available in the literature (Courtney, 1995) [13]. It is clear that the force field that exists inside the mill is quite complex and for this reason predicting the motion of the grinding media is not a trivial task. Nonetheless, using the discrete element method (DEM) this complex motion could be visualized (see Mishra, 1995 [14]; Cleary and Hoyer, 2000 [15]).

The DEM was first proposed by Cundall and Strack (1979) [16] for simulating behaviour of a system of discrete interacting bodies. This scheme is used here to predict the motion of balls in a planetary mill. The discrete element modeling starts with a description of elements or entities comprising the physical system. In a two-dimensional representation, these elements could be simply line-type or disc-type or both. A proper contact detection scheme is required depending on the shape of these elements. Knowing the contacts for any given element and its relative displacement, the force balance equations of DEM are solved. These are the translation and rotational equations of motion, and contact deformational equation. In the case of damping, additional terms defining the damping behavior of the material may be incorporated into the contact deformational equation. These equations are presented below in their most compact form as

$$M\frac{d^2x}{dt^2} + C\frac{dx}{dt} + Kx = p \quad (1)$$

where M, C and K may be considered as the mass, damping, and stiffness matrix, respectively; p is the applied force vector and x is the position vector. Equation (1) describes the motion of a system of particles. where the internal restoring forces are due

to a pair of springs acting at contact in both normal and shear directions. In addition, pair of dashpots at contact point damps the forces. Coefficient of friction plays a role at the contact where the absolute value of the force in the shear direction is never allowed to increase beyond a limiting value given by the product of normal force and coefficient of friction. In the DEM formulation of a planetary mill, the force balance is modified to take into account the Coriolis acceleration. The motion of balls is computed by integrating equation (1) by a central difference method where the incremental displacements are computed at every time step. The central difference scheme as used in DEM is conditionally stable. The limit on the time step for integration is therefore set at:

$$\Delta t \leq \frac{2}{\varpi_{\max}}.$$

The main calculation is done under a time-increment loop, and since DEM analysis requires tens of thousands of time steps, an efficient contact detection algorithm is required. Once one element's contacts with other elements are established, the next task is to compute relative velocity between the contacting elements. From the relative motion of neighboring elements and the interaction relationships, contact forces between these elements are computed. These contact forces are then computed for all of the neighboring contacts and are summed for each element. Applied forces resulting from environmental conditions such as buoyancy, drag or adhesive forces are also computed for each element. By stepping in time, the motion of the elements is computed from dynamic equilibrium equation. The entire solution procedure is repeated for the next time step after updating the coordinates and potential neighboring contacts for each element. A detail description of the numerical method is reported elsewhere (Mishra, 2003) [17].

3.2 Numerical result

In this numerical study, a 13.5 cm diameter mill situated on a 750 mm gyration shaft is simulated to study the charge motion during one revolution of the gyrating shaft. The mill is loaded with balls of 6 mm diameter, which fills the mill to 30% including charge porosity. For this mill it is found that the ratio of mill speed to gyration shaft speed, *R*, must lie within the range –3.36 to 1.36. During one revolution, snapshots were taken at equal intervals of time, and the result of simulation at 60 % of critical speed is shown in Fig. 2. Here the mill rotates in clockwise direction, and accordingly the main shaft rotates in opposite direction. As seen from the figure the charge within the mill is displaced in the direction of the motion of the mill.

4. EXPERIMENTAL

Starting materials used for milling were silicon and graphite with 99.5 and 99% purity respectively. Silicon and graphite were mixed in 1:1 atomic ratio. Milling was carried out for 40 hours in two jars—each containing 125 gm powder and 2.5 kg steel balls. Steel balls of diameter 6 and 12 mm were used for milling. To prevent agglomeration a dispersant known as Licowax was used (1% by weight). The mill was run continuously for 5 hours. When the temperature of the jar comes to room temperature the jar was opened. A small amount of powder was taken from the jar for analysis. The powder samples were analyzed at different intervals of milling time to study the progress of reaction. Powder particles were characterized by X-ray diffraction (CuK_{α}), laser particle size analyzer (Malvern), Raman spectroscopy (Renishaw), scanning electron microscope

(FEI Quanta) and transmission electron microscope (PHILIPS). The samples of TEM have been prepared by mixing the powders with a small amount of pure alcohol and stirring 30 minutes. Two or three drops of the suspension were placed on a carbon coated Cu grid and then well dried for 10 minutes before mounting the grid onto the TEM sample holder.

4.1 Preparation of Al- SiC composite

By froth flotation technique unreacted graphite was separated from bulk powder that was obtained after 40 hours of milling. The concentrate and the tailing fractions were allowed to dry in an oven. The tailing that mostly contained silicon carbide particles was subjected to further separation using a heavy liquid (density 2.6 gm/cc). The float and sink fractions contained silicon and silicon carbide particles respectively. The overall yield after the separation processes was calculated to be 66%. The silicon carbide powder was mixed with aluminum powder for the synthesis of Al-SiC metal matrix composite. SiC powder at 10 and 20 vol.% were mixed with Al powder and pellets were prepared by cold compaction. The cold compacted pellets were then sintered at 400, 500 and 600°C for 1 hour to study the mechanical property. In order to study the effect of sintering temperatures and addition of volume fraction of SiC, Vickers micro hardness measurements were carried out using 160 microhardness tester, (Carl Zeiss, Jena, Germany.) A test load of 20 gm was applied for 10 seconds. The scanning electron microscope (SEM) with the built in energy dispersive spectroscopy (EDS) was used to study the morphology of particles.

5. CHARACTERIZATION OF THE SiC POWDER

5.1 Phase transformation

In order to determine the phase change of the particle mixtures during the reaction milling process, a small sample of milled product was repeatedly picked up at regular intervals for X-ray diffraction analysis. Figure 3 shows the XRD graph of powder milled for 40 hours. The two different X-ray patterns correspond to milled powder prepared by using 6 and 12 mm diameter steel balls. In either spectrum the peaks corresponding to Si_5C_3, SiC and βSiC are present. However, the intensity of silicon carbide peaks is higher corresponding to the powder that was processed with 12 mm diameter steel balls as compared to the powder processed by 6 mm balls under identical conditions. At the end of the experiment, it was also observed that the 6 mm balls were invariably found coated with the powder whereas no such coating was observed on the 12 mm balls. This shows that the intensity of impact in case of 12 mm diameter ball is sufficient to dislodge any coating that forms on the surface of the ball.

The XRD patterns of the end product (as milled SiC powder) are shown in Fig. 4 for different intervals of milling time. Several interesting observations are made. First, the graphite peak disappeared after about 10 hours of milling. This is a general observation in this study, which may be due to amorphization of graphite during milling. However, at this stage the disappearance of the graphite peaks was not accompanied by a shift in the silicon peaks, which indicate that there was no formation of Si(C) solid solutions. In fact, the shifts in the peaks would have suggested that a transitional bonded state between Si and C formed, although no trace of SiC was observed. Second, with increased milling time, silicon peaks also disappeared and silicon carbide peaks were observed. The silicon peak disappeared around 20 hours of milling. Finally, as evident from Fig. 4, the Bragg

peaks for the milled product (after about 40 hours of milling) are broad, suggesting accumulation of lattice strain and reduction in crystallite size. These two individual contributions to broadening have been analyzed in the next section.

5.2 Crystal size and lattice strain

Some features of the activation process, particularly the crystal size, can be investigated by analyzing the X-ray diffraction pattern. For this purpose, as received and milled powders were analyzed using X-ray diffraction (XRD) methods with CuK_α radiation. The XRD peak broadening was used to measure the particle size and internal strain. The broadening due to small crystal size was evaluated through Scherrer formula

$$B_p(2\theta) = \frac{0.9\lambda}{D\cos\theta}$$

where D is the average crystal size, $B_p\ (2\theta)$ is the broadening of the diffraction line measured at full width half maximum intensity (FWHM), λ is the wave length of the x-ray radiation and θ is the Bragg angle. The strain broadening can be calculated as

$$B_s(2\theta) = 4\eta\frac{\sin\theta}{\cos\theta}$$

where $B_s\ (2\theta)$ is the broadening due to internal strains and η is the effective internal strains. The total broadening, $B_t\ (2\theta)$, due to both the crystal size and internal strains was assumed to be the linear addition of the two contributions. From the slope and the intercept of the plot of $B_t\cos\theta$ versus $\sin\theta/\lambda$, the crystallite size and internal strain were

calculated. Correction for instrumental broadening, which comes due to the superposition of peaks due to $K_{\alpha 1}$ and $K_{\alpha 2}$, when peaks are not resolved, was taken into account in the measurement of the peak broadening. This was done by running XRD of pre-milled powder under the same conditions as the milled powder. The breadth at half maximum intensity (FWHM) of the desired curve B_t (2θ), which could be obtained if there were no instrumental broadening, was calculated by linear subtraction of breadth of before milled powder from total breadth.

The decrease of the grain size and lattice strain to characterize the activation process has been determined from the X-ray diffraction patterns. Although the accumulation of lattice strain is a measure of defect formation, determining the defect structure was found to be more difficult. The crystallite size and the lattice strain of the powder measured from the XRD peak broadening is shown as a function of milling time in Fig. 5. It can be seen that the crystallite size decreases and internal strain increases rapidly with milling time up to about 20 hours. With further milling the crystallite size remains almost constant but internal strain appears to decrease. This could be the onset of phase change (i.e., nucleation of SiC). Finally, from Fig. 5 it is noticed that the different mass of the balls results in different crystal size and strain accumulation rates.

5.3 Particle size

During the early stage of milling, the powder particles of Si and C are mixed together and then mechanically activated such that individual particles of Si and C could form composite particles. At a later stage, after about 20 hours of milling, the solid-state reaction starts and considerable amounts of the product (SiC) are formed. Fig. 6 shows the particle size distribution of powder at different intervals of milling time. While the d_{25}

(25% passing size) size continuously decreased from 10 to 1 micron, the d_{75} size decreased from 25 to 15 micron. Similar experiments under identical conditions with 12 mm balls produced a coarser particle size distribution after 40 hours of grinding. However, the rate of SiC formation during milling was better with 12 mm ball.

There was no evidence of welding, as particle size did not increase during the initial stages of milling. It should be mentioned that the size spectra corresponding to individually milled product of Si and C did not show any evidence of growth in particle size. In contrast, in TiC system, El-Eskandarany (1996) [18] analyzed the polished and etched particles representing the early stage of grinding. They showed that the individual particle contains many thick layers of the diffusion couples of constituent powders. They believed that a solid-state reaction occurred at the clean-interfaces of these layers, and a new single phase was formed after further milling. When the new phase formed the reactant layers disappeared. Therefore, in such systems the only way the particles could grow is by cold welding. However, similar mechanism of phase formation was not observed in the SiC system.

5.4 Raman spectra analysis

The Raman spectra were recorded by using the 514-nm radiation of an Ar laser excitation. The characteristic Raman spectra of 40 hours milled final powder are shown in Fig. 7. The spectra show mainly two sharp and strong peaks at 781 and at 970cm^{-1}, and a weak broad peak at 1504. The two strong peaks at 781 and 970 correspond to SiC, while the weak broad peak corresponds to graphite. So it is believed that some unreacted graphite is present with SiC. But Raman spectrum does not show the presence of any unreacted Si. Ricciardi et al. (2005) [19] studied Raman spectroscopy of polycrystalline

3C-SiC thin film on Si substrate. They showed strong spectra at 520 cm^{-1} due to Si substrate, and two spectra at 795 and at 974cm^{-1} for polycrystalline 3C-SiC.

5.5 Temperature

The temperature of outer surface of the jars during milling was measured by a high precision laser pyrometer. The temperature measurements were carried for a total period of 5 hours. During this period milling was carried out continuously. It was observed that after about 3 hours of grinding a steady state condition was attained when the temperature remained constant. The variation in the measured temperature of the outer surface of the jar during milling is shown in Fig. 8. Here the temperature profiles correspond to milling of pure graphite and silicon carbide (Silicon and graphite). It is clear from the figure that the outer surface temperature reach 90 and 75 ºC during SiC and graphite milling respectively. Under the steady state condition, the temperature of the inner surface of the jar was calculated by a simple heat balance. The measured temperature of the outer surface of the jar and calculated temperature of the inner surface of the jar for different materials are presented in Table 1.

The actual processing of the powder takes place during the collisions between two balls or a ball and the wall of the mill. From the point of view of reaction milling, a particularly important question is the temperature increase during collision. The possible approaches were reviewed by Koch (1994, 2003) [20] and recently worked out in some detail by Murty et al (2004) [21]. Depending on the model, rather different estimates of the temperature increase were obtained. For example, when Fe powder was impacted by an 8-mm steel ball, the inner wall temperature was estimated to be 150ºC. These

temperatures appear to be sufficient for chemical reaction given the state of mechanical activation achieved in the planetary mill.

5.6 Scanning electron microscopy (SEM)

The SEM was used to follow the changes in the shape and the size of the milled powders during different stages of the reaction milling process. Fig. 9 shows the SEM micrographs of the milled powders after different intervals of milling time. In all the micrographs the marker is set at 50 micron. At the initial stage of milling, the powders of the reactant materials are bulky, with random shape and size. As the milling progressed the powders became spherical as evident from Fig. 9(d), which correspond to 40 hours of milling. As regards particle size, it is also evident from the SEM images that it decreases gradually with increasing milling time. However, no evidence of particle coarsening could be obtained through SEM.

5.7 Transmission electron microscopy (TEM)

The internal structure of the reaction milled powder after 40 hours was analyzed by the TEM. Fig. 10 shows the bright field TEM micrograph and the corresponding SAD pattern. The micrograph shows that the particle size ranges from 100 to 300 nm. The EDS spectrum shows the peaks of Si, C and Fe. Fe is the contaminant, which comes from the surface of the steel jar and balls during milling. The spot pattern was obtained for individual Si_5C_3 grains. Fig. 11 shows another bright field TEM micrograph and the corresponding SAD pattern. The schematic of SAD pattern is also shown in the figure. The micrograph shows that two deformed crystals are present. The crystals are quite large and around 2μ thick. The SAD pattern is a diffraction of double diffraction i.e. diffraction come from two crystals.

6. CHARACTERIZATION OF Al-SiC COMPOSITE

6.1 Scanning Electron Microscopy (SEM)

To study the morphology and distribution of silicon carbide particles in the Al matrix, SEM was used. Fig. 12 shows the SEM picture and the EDS spectra of Al-10 vol.% SiC composite that was sintered at 600°C in an inert atmosphere for 1 hour. The micrograph shows that SiC particles are agglomerated and non-uniformly distributed in the Al matrix. The EDS of embedded particle shows Si and Fe while the matrix shows only Al as major constituents. This indicates that the SiC powder is contaminated with Fe that was generated during milling as a product of wear of steel balls and liner. Interestingly, the contamination due to Fe was not evident from the X-ray diffraction data.

The SEM micrograph shows good compatibility between Al matrix and SiC particles. It shows good interfacial bond between Al matrix and SiC particles, no voids or cracks are present. The interface between the metal and the particle plays a critical role in determining the overall properties of metal matrix composites. Strengthening by the hard particle reinforcement depends critically on the interfacial bond. A well-bonded interface facilitates the efficient transfer and distribution of load from matrix to the reinforcing phase, which lead to improved composite strengths as reported by Lin et al. (1990) [22]. Conversely, load transfer becomes less effective with a weak bond, limiting the amount of strengthening that can take place. Therefore, it is concluded that a strengthened interfacial bond is responsible for the improvement in mechanical properties.

From SEM micrographs, it is also clear that the interfaces were very clean; no precipitation of interfacial Al_4C_3 was formed. The reacted layer which is formed at the interface is also very important. The reacted layer composed of the brittle Al_4C_3, its

fracture strength is controlled by these intrinsic defects as studied by Lee et al. (1994) [23]. Tham, Gupta et al. (2001) [24] studied the effect of matrix-reinforcement interfacial reaction on the enhancement of mechanical properties of Al-SiC composites. It is commonly supposed that the reaction layer itself constitutes a flaw, in the form of a through-thickness crack, and since the size of the flaw is dictated by the thickness of the reacted layer, thicker layers are more prone to fracture because they have a greater statistical probability of containing flaw that is larger than a certain critical size.

6.2 Elemental mapping

Elemental mapping was used for displaying information about the distribution of a single element. Fig. 13 shows elemental mapping of Al and Si for Al-10 vol.% SiC composite sintered at 600°C for 1 hour in inert atmosphere. It shows the distribution of major components like Al and Si in the matrix and second phase particles respectively. No reacted product of amorphous or an intermediate phase can be identified, by segregation of the elements of Al and Si in the composite sample.

6.3 Density and hardness study

Densities of Al-10vol.% SiC and Al-20vol.% SiC composites were calculated by measuring physical dimensions and taking weight in electronic balance. Here 90% of theoretical density was achieved. With increasing temperatures there was no improvement of density.

The effect of various sintering temperatures and the effect addition of SiC, on Al-SiC composites were studied. Vickers microhardness tests were thoroughly studied. Total test load of 20 gm applied for 10 seconds. A minimum of 3 measurements were taken for each specimen. Fig. 14 shows the variation of hardness with temperatures and volume

percent of SiC. The figure shows that hardness of Al-SiC composite is higher than pure Al at all temperatures. It also shows that hardness increases with increasing sintering temperatures. Tham et al. (2001) [24] synthesized Al-SiC composites, which essentially involves incorporating the SiC particles by mechanically stirring the fully molten aluminum alloy with an impeller as the particles are added. They measured microhardness of composites and showed matrix hardness of about 36 ± 2 and 39 ± 1 depending on the contact time of molten Al and SiC particles. Here maximum microhardness of about 40 for Al-20 vol.% SiC composite sintered at 600°C for 1 hour was obtained which is very close to the previous study.

7. CONCLUSIONS

Silicon carbide has been synthesized in a specially built dual drive planetary mill using the concept of reaction milling. It was found that 12 mm balls enhances intensity of impact which was evident from the quality of powder and lattice strain rates attained during processing. However, particle size distribution was found to be coarser when the milling was carried out using 12 mm balls. At the end of 40 hours of milling, SiC of crystallite size 10 nm was formed and the powder contained 20% less than one micron. Unlike the commercially available planetary mills where it takes 300 hrs to obtain SiC, the dual drive planetary mill produces the same in about 40 hours. The composites made out of SiC and Al shows that the interface is sharp and clean (i.e., precipitate and reaction

free), no voids or cracks are present. With increasing sintering temperature hardness of Al-SiC composites increase due to good compatibility between Al and SiC particles.

8. REFERENCES

1. Vogt, G.J., Vigil, R.S., Newkirk, L.R., and Tukula, M., Proc. Of the 7th International Symp. On plasma Chemistry, Vol. 2, ed. Timmermans, C.J, Eindhoven, H, International Union of Pure and Applied Chemistry, 1985, p. 668.

2. Cannon, W.R., Danforth, S.C., Flint, J.H., Haggerty, J.S., and Marra, R.A., "Sinterable ceramic powders from laser-driven reactions - 1. Process description and modeling". J. Am. Ceramic Soc., 65 (1982) 324-330.

3. Cannon, W.R., Danforth, S.C., Haggerty, J.S., and Marra, R.A., "Sinterable ceramic powders from laser-driven reactions - 2. Powder characteristics and process variables", J. Am. Ceramic Soc., 659 (1982) 330-335.

4. Ritter, J. J., in Better ceramics through Chemistry II, Materials Research Society Symp. Proc., Vol. 73, eds. Brinker, C.J., Clark, D.E., and Ulrich, D.R, Materials Research Society, Pittsburgh, PA, 1995, p. 367.

5. Le Caer, G., Bauer-Grosse, E., Pianelli, A., Bouzy, E., and Matteazzi, P., "Mechanically driver syntheses of carbides and silicides", J. Mater. Sci., 25 (1990), p. 4726–4731.

6. Matteazzi, P., and Caer, G. L., "Room temperature mechano-synthesis of carbides by grinding of elemental powder", Journal of American Ceramic Society, 74 (6), 1991, p.1382-1390.

7. El-Eskandarany, M.S., Sumiyama, K., Suzuki, K., “Mechanical solid state reaction for synthesis of β-SiC powders”, Journal of Materials Research, 10: (3), 1995, 659-667.
8. Yang, Z.G., and Shaw, L.L., “Synthesis of nanocrystalline SiC at ambient temperature through high energy reaction milling”, Nanostructured Materials, Vol. 7, No. 8, 1996, p. 873-886.
9. Schwarz, R.B., and Petrich, R.R., “Calorimetry study of the synthesis of amorphous Ni-Ti alloys by mechanical alloying”, Journal of Less-common Metals, 140, 1988, p.171-184.
10. Schwarz, R.B., Petrich, R.R., and Saw, C.K., “The synthesis of amorphous Ni---Ti alloy powders by mechanical alloying ”, Journal of Non-Crystalline Solids, 76 (2-3), 1985, 281-302.
11. McCormick, P.G., and Froes, F.H., “The fundamentals of mechanochemical processing.” Journal of Metals, 50 (11), (1998) p. 61-65.
12. Rajamani, R. K., Milin, L., Howell, G., “Dual drive planetary mill” 2000, United States Patent no. 6,086,242.
13. Courtney, T.H., “Process modeling of mechanical alloying (overview)”, Mater. Trans. JIM, 36 (1995) 110.
14. Mishra, B.K., “Ball charge dynamics in a planetary mill.” KONA No. 13, (1995) p.151-158.
15. Cleary, P.W., Hoyer, D., “Centrifugal mill charge motion and power draw: comparison of DEM predictions with experiments”, International Journal of Mineral Processing, 59, 2000, p.131-148.

16. P.A. Cundall, O.D.L. Strack, “A discrete numerical model for granular assemblies, Geotechnique 29, 1979, pp. 47-65.
17. Mishra, B. K., “A review of computer simulation of tumbling mills by the discrete element method: Part I – contact mechanics and part II – practical applications”, International Journal of Mineral Processing, 71, 2003, pp. 73-93 and pp. 95-112.
18. El-Eskandarany, M.S., “Synthesis of nanocrystalline titanium carbide alloy powders by mechanical solid state reaction”, Metall. Trans. A, 27, 1996, p. 2374-2382.
19. Ricciardi, C., Giorgis, F., Fanchini, G., Musso, S., Ballarini, V., Bennici, E., Barucca, G., Rossi, A.M., “Microstructure analysis on polycrystalline 3C-SiC thin films”, Diamond & Related Materials, 14, 2005, pp. 1134-1137.
20. Koch, C.C., “Top-down synthesis of nanostructured materials: Mechanical and thermal processing methods”, Rev. Adv. Mater. Sci., 5, 2003, p. 91–99.
21. Joardar, J., Pabi, S.K., and Murty, B.S., “Estimation of entrapped powder temperature during mechanical alloying” Scripta Materialia, 50(9), 2004, p.1199-1202.
22. Lin, Y. R., Kannikeswaran, K., in “Interfaces in Metal-Ceramics Composites”, Ed. Lin., Y. R., Arsenault, R. J., Martins, P. G., and Fishman, G. S., TMS, Warraendale, Pa, 1990, p. 53.
23. Lee, j. C., Ahn, J. P., Shim, J. H., Shi, Z. and Lee, H. I., “Control of the interface in Al/SiC composites”, Scripta Materialia, 41 (1999) 895.

24. Tham, M. L., Gupta, M., and Cheng, L., “Effect of limited matrix-reinforcement interfacial reaction on enhancing the mechanical properties of Aluminum-Silicon Carbide composites”, Acta Materialia, Vol. 49 (2001), p. 3243-3253.

List of figures

Figure 14. Hardness of Al-SiC composites and pure Al sintered at different temperatures for 1 hour.

List of Tables

Table 1. Inside and outside vial surface temperature for different materials.

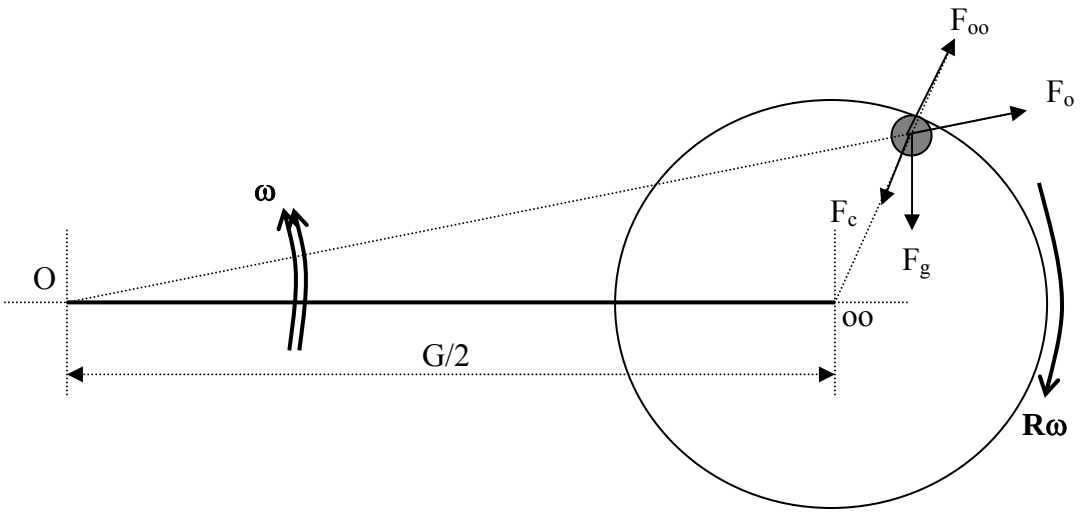

Figure 1. Schematic of the acceleration field in a planetary mill.

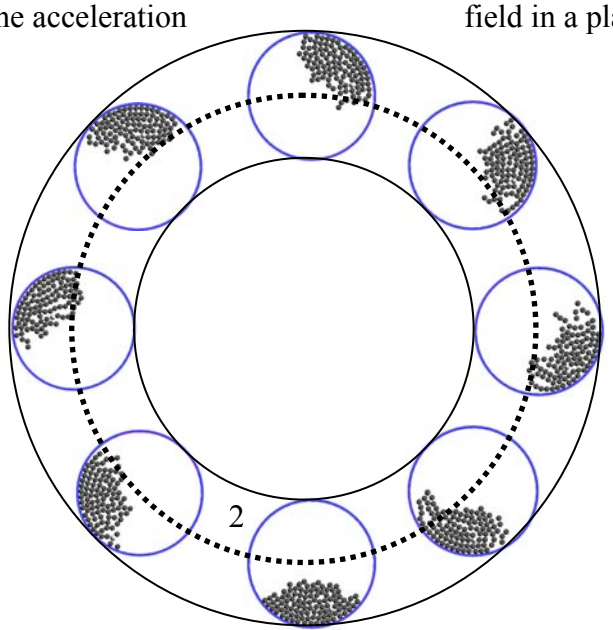

Figure 2. Charge motion inside planetary mill at 60% critical speed.

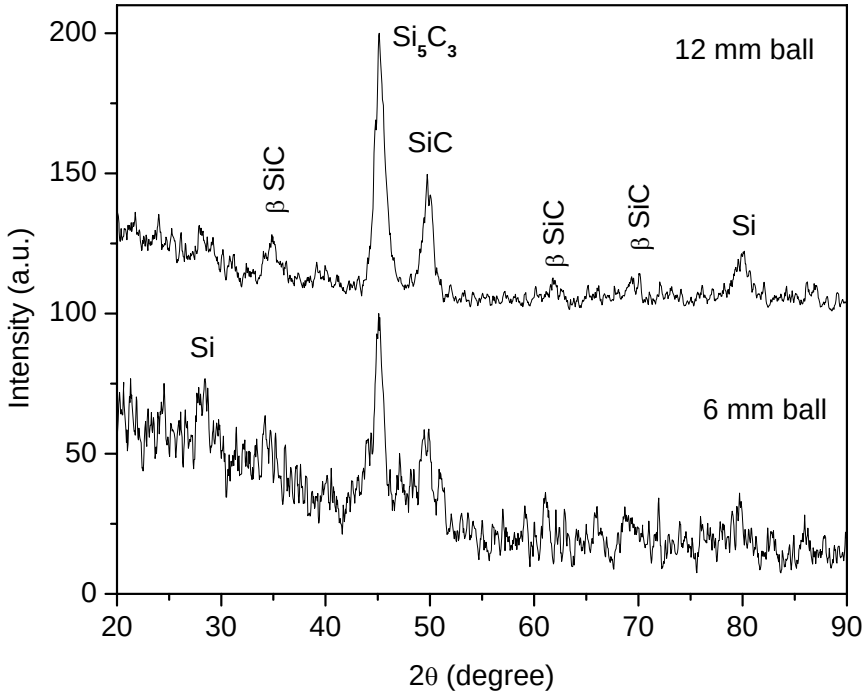

Figure 3. XRD patterns of milled powder at 40 hours of milling times for two different size balls.

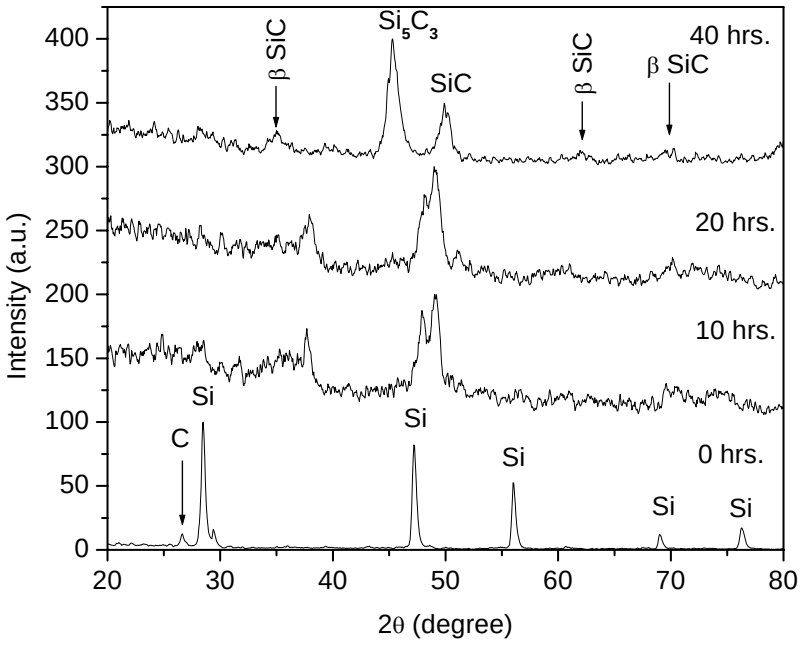

Figure 4. XRD patterns of milled powder at selected milling times.

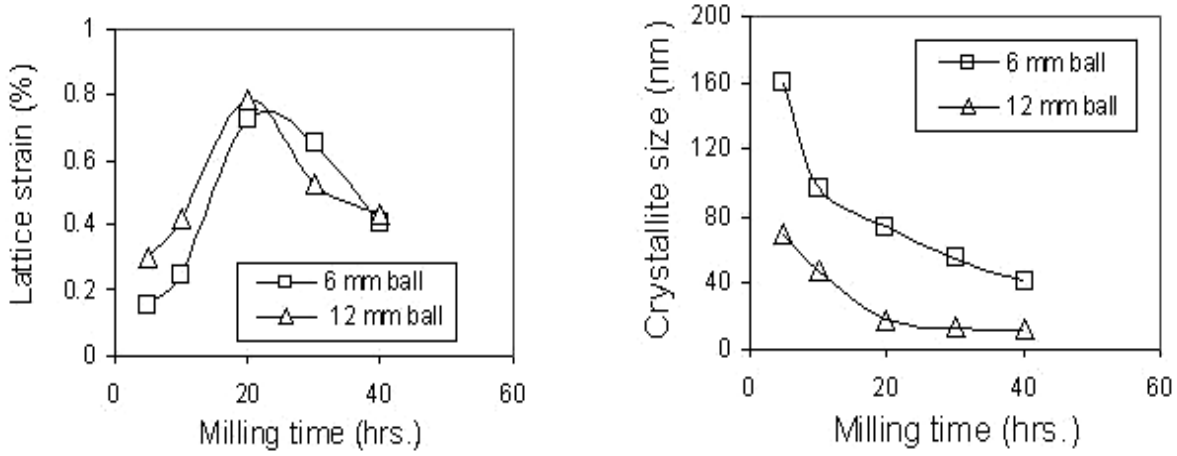

Figure 5. Effect of ball size on lattice strain and the crystallite size of the milled powder calculated from X-ray diffraction patterns; left: lattice strain; right: Crystal size.

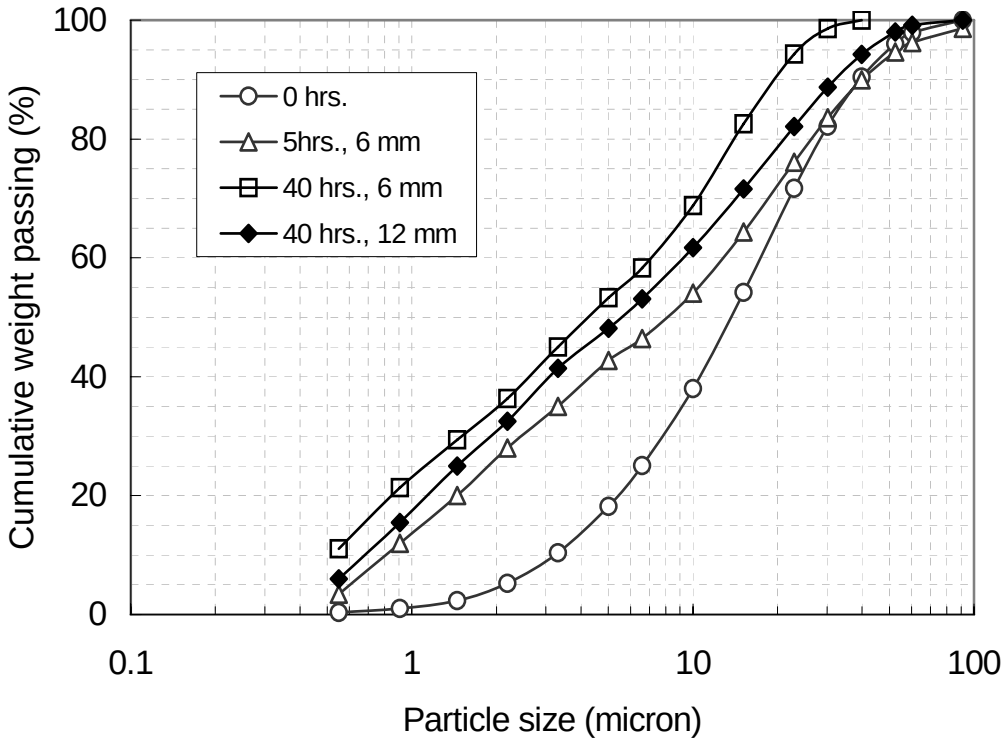

Figure 6. Particle size distribution of the milled product at different intervals of time.

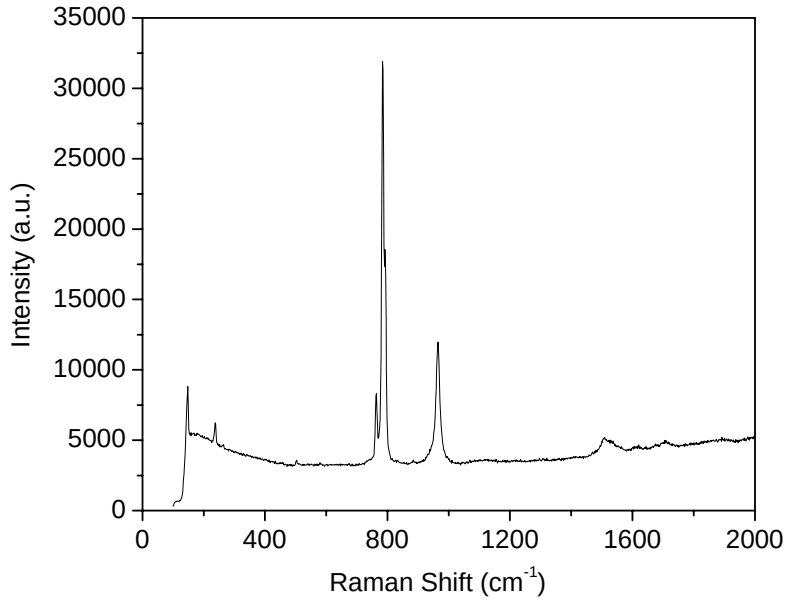

Figure 7. Raman spectra of 40 hours milled final powder.

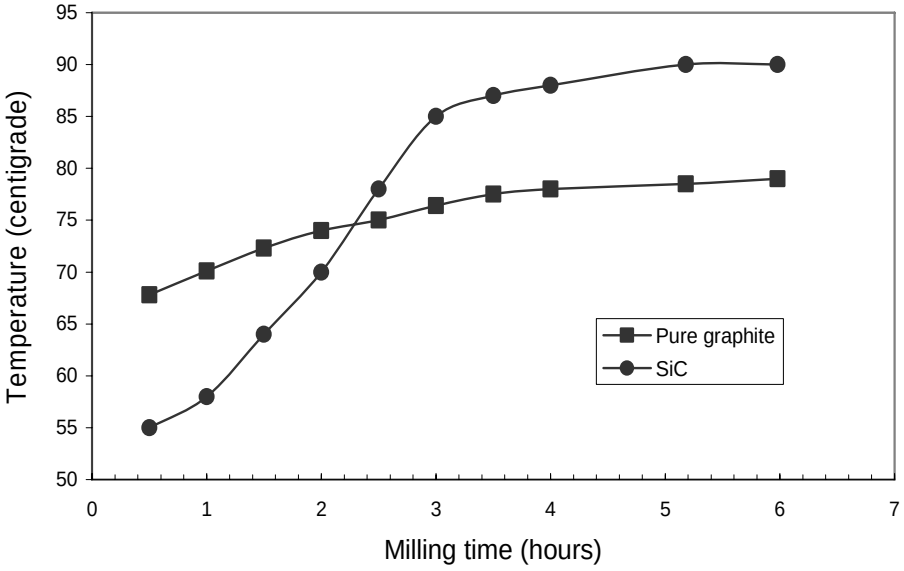

Figure 8. Rise in temperature of the outer surface of the jar.

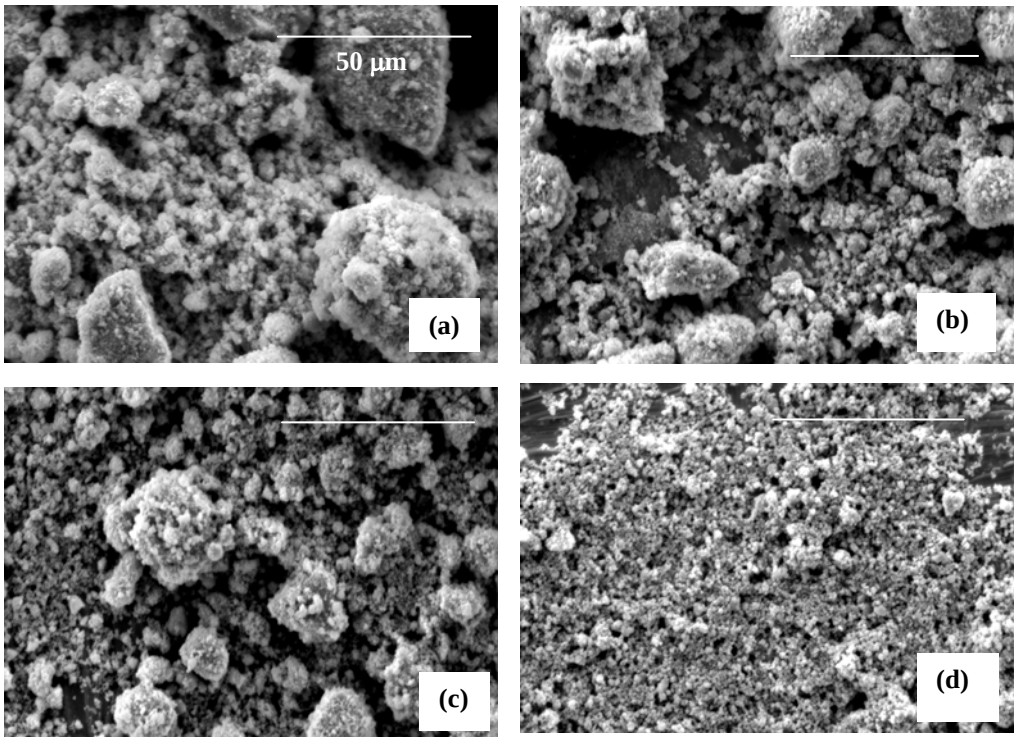

Figure 9. SEM photograph of the powder after (a) 10 (b) 20 (c) 30 and (d) 40 hours of milling.

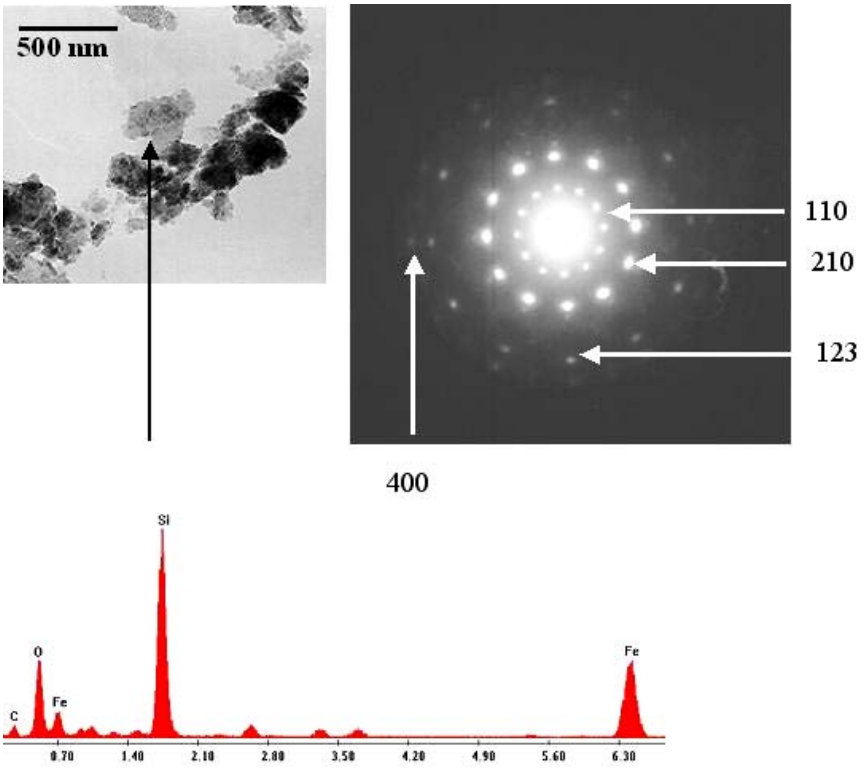

Figure 10. Bright field TEM micrograph and corresponding SAD pattern. The EDS spectrum of a particle is also shown in the figure.

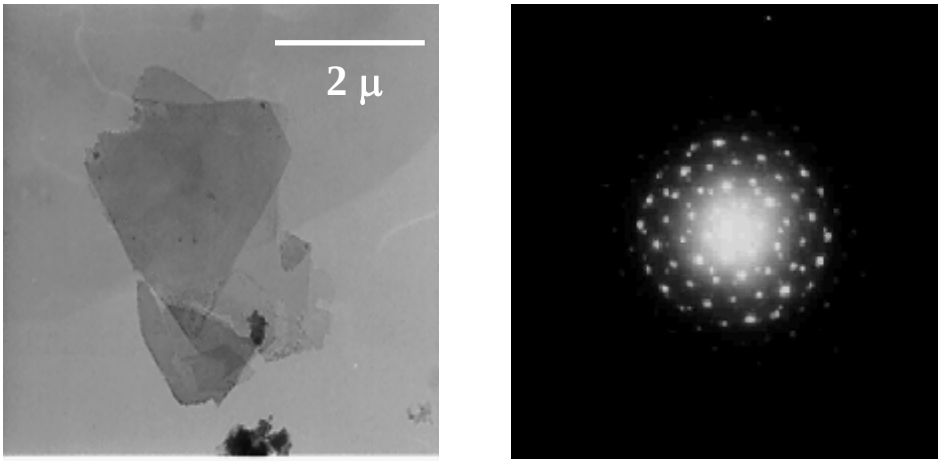

(a) (b)

Figure 11. (a) Bright field TEM micrograph and (b) corresponding SAD pattern

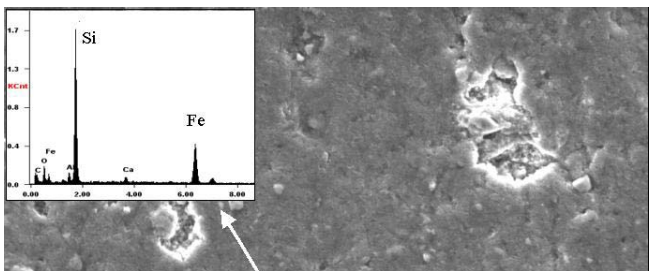

Figure 12. SEM picture and EDS spectra of the Al-10 vol.% SiC composite sintered at 600°C in an inert atmosphere for 1 hour.

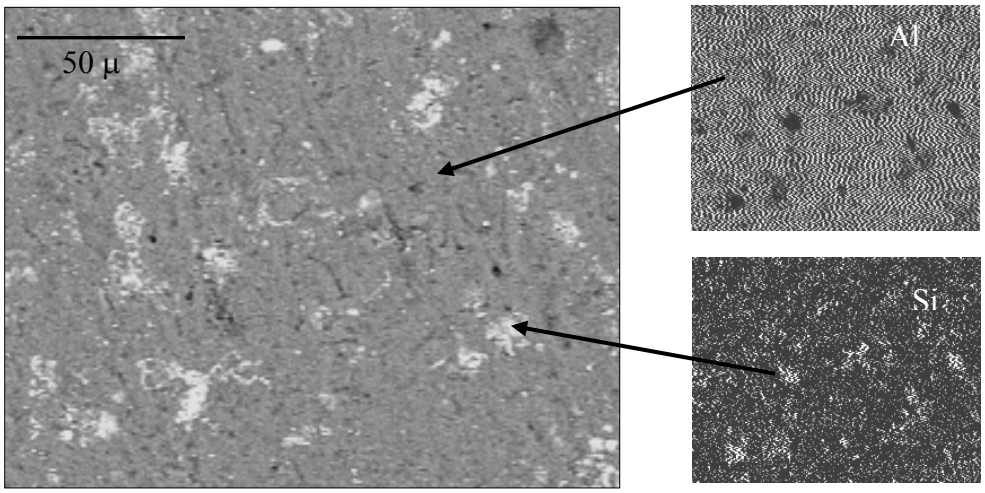

Figure 13. Elemental dot mapping of Al-10 vol. % SiC sintered at 600°C for 1 hour in inert atmosphere.

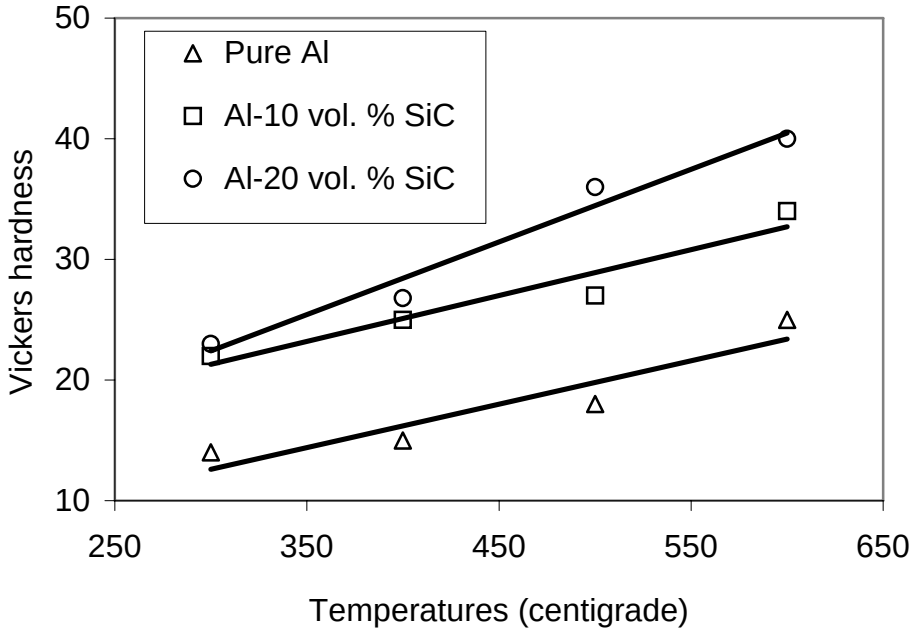

Figure 14. Hardness of Al-SiC composites and pure Al sintered at different temperatures for 1 hour.

Table 1. Inside and outside vial surface temperature for different materials.

Materials	Measured outside temperature (°C)	Calculated inside temperature (°C)
Pure iron	116	150
Pure graphite	79	113
Iron + graphite (C: Fe = 1.5)	93	127
Iron + graphite (C: Fe = 2.0)	83	117
SiC	90	124
Limestone	85	119